

Comparison of methods for processing acoustic intensity from orthogonal multimicrophone probes

Curtis P. Wiederhold

Department of Mechanical Engineering, Brigham Young University, Provo, Utah 84602

Kent L. Gee

Department of Physics and Astronomy, Brigham Young University, Provo, Utah 84602

Jonathan D. Blotter^{a)}

Department of Mechanical Engineering, Brigham Young University, Provo, Utah 84602

Scott D. Sommerfeldt

Department of Physics and Astronomy, Brigham Young University, Provo, Utah 84602

(Received 8 August 2011; revised 10 February 2012; accepted 14 February 2012)

One design for three-dimensional multimicrophone probes is the four-microphone orthogonal design consisting of one microphone at an origin position with the other three microphones equally spaced along the three coordinate axes. Several distinct processing methods have been suggested for the estimation of active acoustic intensity with the orthogonal probe; however, the relative merits of each method have not been thoroughly studied. This comparative study is an investigation of the errors associated with each method. Considered are orthogonal probes consisting of matched point sensor microphones both freely suspended and embedded on the surface of a rigid sphere. Results are given for propagating plane-wave fields for all angles of incidence. It is shown that the lowest error for intensity magnitude results from having the microphones in a sphere and using just one microphone for the pressure estimate. For intensity direction, the lowest error results from having the microphones in a sphere and using Taylor approximations to estimate the particle velocity and pressure. © 2012 Acoustical Society of America. [<http://dx.doi.org/10.1121/1.3692242>]

PACS number(s): 43.58.Fm, 43.20.Fn [DKW]

Pages: 2841–2852

I. INTRODUCTION

Active intensity is an acoustic energy quantity useful in characterizing sound fields. One important application is its use in sound source localization. To calculate this quantity at a given point in space, the pressure and particle velocity at that point must be simultaneously known. The pressure can be estimated using a finite sum between two or more microphones and the velocity with a finite-difference calculation—a method known as the p-p technique.^{1–3} This is in contrast to the p-u technique, wherein the particle velocity is measured directly.^{4,5} With two microphones, the intensity can be estimated in one dimension, whereas with four or more microphones it is possible to get a complete three-dimensional estimation.⁶

Such probes, also capable of estimating energy density, are referred to as multimicrophone probes (alternatively known as vector probes, intensity probes, or energy density sensors) and have been in wide use since the 1980s. The three most common designs of multidimensional, multimicrophone probes are the four-microphone orthogonal design,^{7,8} the four-microphone regular tetrahedron design,^{9–11} and the six-microphone design.^{6,12} In this work the four-microphone orthogonal design will be investigated by comparing the various implementations of this probe design in estimating intensity.

As shown in Fig. 1(a), the orthogonal design consists of one microphone at an “origin” position (labeled microphone 1) with the other three microphones (labeled 2–4) equidistant from the first microphone along the three coordinate axes. It has previously been referred to as the “cubic” probe,^{13,14} but “orthogonal” is preferred here because the probe does not consist of microphones at all the vertices of a cube.

Many multimicrophone probes consist of microphones suspended in space near each other, with acoustic scattering avoided by making the microphone-holding fixture as small as possible.^{15,16} Such probes are typically analyzed assuming that the microphones are point sensors freely suspended in space, thus neglecting any effects from scattering.^{8,14} It has alternatively been suggested that the microphones be embedded on the surface of a hard sphere, a situation where the scattering is predictable.¹⁷ It was shown that, for a two-microphone case, having the sensors embedded in a sphere results in slightly less error in measuring acoustic quantities in both active and reactive fields when the microphone responses are matched. However, when phase and amplitude mismatch are introduced, the effect is lost and the errors are dominated by the mismatches. But in both cases (with matched or mismatched microphones), the spherical scattering effectively allows for the physical microphone separation distance in spherical probes to be made more compact by a factor of 2/3 with equal low-frequency error.^{12,17} Due to the benefits resulting from the spherical scattering, a spherical orthogonal probe design has been suggested and a prototype has been made, resulting in a probe as shown in

^{a)}Author to whom correspondence should be addressed. Electronic mail: jblotter@byu.edu

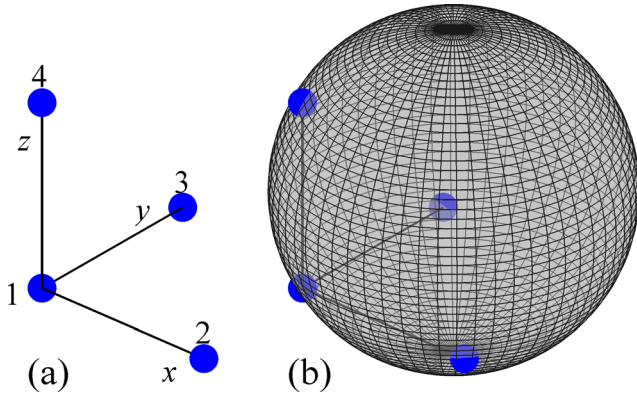


FIG. 1. (Color online) Four-microphone orthogonal probe designs with microphones freely suspended (a) and mounted on the surface of a sphere (b). Dots represent microphone locations.

Fig. 1(b).¹⁸ Although work has been done for the two-microphone case,^{12,17} a thorough study has not been done to investigate whether mounting the microphones on a sphere (spherical scattering) or having them freely suspended (assuming no scattering) results in more accurate measurements for orthogonal probes. In this paper, results from a rigid sphere probe design will be compared to those from a freely suspended probe design.

The various processing methods used to estimate the intensity vector using an orthogonal multimicrophone probe along with the consideration of whether or not to mount the microphones on a sphere lead to 16 intensity calculation combinations considered in this paper. Section II outlines the various processing methods used with the orthogonal probe and Sec. III presents the cross-spectral formulas that correspond to each processing method. The model that is used to compare the methods is described in Sec. IV, results are presented and discussed in Sec. V, and concluding remarks are given in Sec. VI.

II. INTENSITY ESTIMATION METHODS

Active acoustic intensity is a measure of the net flow of energy carried by an acoustic wave through a unit area. Using complex notation, the time-averaged intensity is given by

$$\mathbf{I} = \frac{1}{2} \text{Re}\{p\mathbf{v}^*\}, \quad (1)$$

where p is the complex pressure, \mathbf{v} is the complex particle velocity vector, the complex conjugate is denoted by an asterisk, and the real part is denoted by “Re.” The various orthogonal probe processing methods arise from different ways to estimate the particle velocity and the pressure in this expression.

A. Particle velocity estimation

There are two ways the particle velocity has been estimated with the orthogonal probe. Commonly, a finite-difference approximation between each of the two-microphone pairs along the x -, y -, and z -axes is used, thereby estimating the

x -, y -, and z -components of the velocity.^{8,14,19,20} This is done by starting with the time-harmonic, linear Euler’s equation (using the $e^{j\omega t}$ time convention),

$$\mathbf{v} = \frac{j\nabla p}{\rho\omega}, \quad (2)$$

where ρ is the air density, ω the angular frequency, and j the imaginary unit. The gradient of the pressure is estimated by a finite-difference estimate between microphone pairs lying along each coordinate axis, resulting in the following particle velocity expression:

$$\mathbf{v} = \begin{cases} v_x \approx \frac{j(p_2 - p_1)}{2h\rho\omega} \\ v_y \approx \frac{j(p_3 - p_1)}{2h\rho\omega} \\ v_z \approx \frac{j(p_4 - p_1)}{2h\rho\omega} \end{cases} \quad (3)$$

with $2h$ being the distance from the origin microphone to any of the three other microphones and p_1 , p_2 , p_3 , and p_4 being the complex pressures at the microphone locations shown in Fig. 1. The systematic method of obtaining least-squares finite-difference estimates described by Pascal and Li¹⁴ gives this expression for the orthogonal probe.

If the microphones are mounted on the surface of a sphere Elko¹⁷ found that the separation distance must be multiplied by a low-frequency correction factor of 3/2. In this case, $3h$ would be used in Eq. (3) instead of $2h$. This correction factor is needed for an accurate low-frequency (approximately $ka < 1$) estimate of the pressure gradient using the finite-difference method. It represents an increased effective distance between the microphones due to the scattering introduced by the sphere and is the reason the spherical probe can effectively be made more compact by a factor of 2/3.

Using Eq. (3) to obtain the particle velocity results in each component of the velocity being estimated at a different point in space and so is referred to in this work as the “three points” velocity estimate. Rasmussen⁶ suggested that this is an important weakness of the orthogonal design. To offset this, Cazzolato and Ghan¹³ have suggested using a weighted pressure estimate to put the point where the pressure is estimated closer to the three points where the velocity is estimated—an idea described more fully in the next section on pressure estimation. Alternatively, Locey¹⁸ has proposed using a first-order Taylor approximation of the velocity utilizing the finite-difference results of all six two-microphone pairs to put the three velocity estimates at one point. With the origin microphone at $(0, 0, 0)$ this method gives an estimate of all three components of the velocity at the point (h, h, h) in the following manner.

The x -component of the particle velocity is approximated as

$$v_x(h, h, h) \approx v_x(h, 0, 0) + h \frac{\partial v_x}{\partial y} \Big|_{(h,0,0)} + h \frac{\partial v_x}{\partial z} \Big|_{(h,0,0)}. \quad (4)$$

The partial derivatives with respect to the y - and z -directions could themselves be approximated by first-order Taylor approximations,

$$\begin{aligned} \left. \frac{\partial v_x}{\partial y} \right|_{(h,0,0)} &\approx \frac{v_x(h, h, 0) - v_x(h, 0, 0)}{h}, \\ \left. \frac{\partial v_x}{\partial z} \right|_{(h,0,0)} &\approx \frac{v_x(h, 0, h) - v_x(h, 0, 0)}{h}, \end{aligned} \quad (5)$$

leading to the final expression

$$v_x(h, h, h) \approx v_x(h, h, 0) + v_x(h, 0, h) - v_x(h, 0, 0). \quad (6)$$

These three terms correspond to velocities estimated at the three points shown in Fig. 2. The x -direction velocity at $(h, 0, 0)$, the midway point between microphones 1 and 2, is calculated using a normal finite difference between those two microphones. However the x -velocity estimates between microphones 2 and 3 and between microphones 2 and 4 require extra calculations because finite differencing between these microphones yields velocities with both x - and y -components (they would point along the directions of the dashed lines in Fig. 2). The problem is overcome by using the velocity information from other pairs of microphones to make an initial estimate of the direction of the velocity. Estimation of $v_x(h, h, 0)$ is used as an example. A diagonal velocity (v_{diag}) between microphones 2 and 3 as shown in Fig. 3 can be calculated at this point using a finite-difference approximation. Then the angle of the three-dimensional particle velocity in the xy -plane can be approximated using the x -direction velocity (obtained from microphones 1 and 2) and the y -direction velocity estimate (obtained from microphones 1 and 3) as

$$\theta_{xy} \approx \tan^{-1} \frac{|v_y(0, h, 0)|}{|v_x(h, 0, 0)|}, \quad (7)$$

where vertical bars give the absolute value of the complex velocity. However, the angle θ_{xy} must be multiplied by a

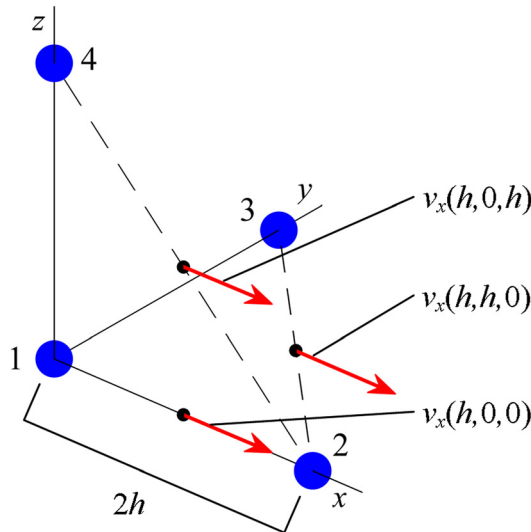


FIG. 2. (Color online) Velocity vectors needed to calculate Taylor approximation of x -direction velocity at point (h, h, h) .

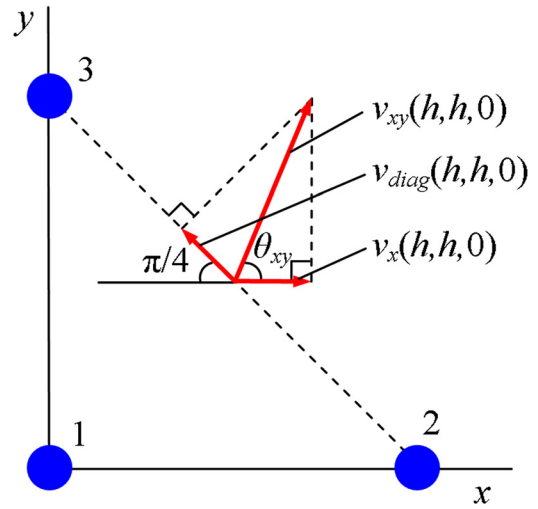


FIG. 3. (Color online) Diagram of method used to estimate x -direction velocity from diagonal velocity.

factor of -1 if the difference in phase between $v_x(h, 0, 0)$ and $v_y(0, h, 0)$ is between $\pi/2$ and $3\pi/2$ radians—that is if

$$\frac{\pi}{2} \leq \left| \arg \left(\frac{v_x(h, 0, 0)}{v_y(0, h, 0)} \right) \right| \leq \frac{3\pi}{2}, \quad (8)$$

where “arg” denotes the angle of the complex number and the vertical bars give the absolute value of the real number. This step is necessary because Eq. (7) uses only the magnitudes of the complex velocities—not enough information to uniquely identify the direction of the acoustic wave. The steps defined in Eqs. (7) and (8) were suggested by Locey as a method to estimate the direction of the plane wave given its orthogonal, complex components. For the plane wave analysis in this paper, Locey’s method appears to work well as defined.

With θ_{xy} and v_{diag} estimated, the x -direction velocity at $(h, h, 0)$ can then be estimated as follows. The velocity v_{diag} is considered to be a component of particle velocity in the xy -plane.

The estimate of this actual velocity in the xy -plane is called v_{xy} and its direction is estimated as θ_{xy} . The velocity $v_x(h, h, 0)$ is then the x -component of the velocity v_{xy} as shown in Fig. 3 and is calculated using

$$v_x(h, h, 0) \approx v_{diag}(h, h, 0) \frac{\cos(\theta_{xy})}{\cos(3\pi/4 - \theta_{xy})}. \quad (9)$$

The final term needed in Eq. (6) to calculate $v_x(h, h, h)$ is the velocity $v_x(h, 0, h)$ and is obtained in a manner similar to $v_x(h, h, 0)$, but in the xz -plane instead. A similar formulation leads to

$$v_y(h, h, h) \approx v_y(h, h, 0) + v_y(0, h, h) - v_y(0, h, 0) \quad (10)$$

for the y velocity and

$$v_z(h, h, h) \approx v_z(h, 0, h) + v_z(0, h, h) - v_z(0, 0, h) \quad (11)$$

for the z velocity. A three-dimensional velocity vector at point (h, h, h) is then fully estimated.

There are thus two ways to estimate particle velocity: First, the typical method of estimating the velocity at three points in space given in Eq. (3) and, second, using a Taylor approximation to put all components of the velocity estimate at the point (h, h, h) via Eqs. (6), (10), and (11).

B. Pressure estimation

To calculate active intensity, pressure must also be estimated. There are five methods to estimate the pressure that are considered in this work. First, the pressure can be estimated as the average pressure of the four microphones,²¹

$$p \approx \frac{p_1 + p_2 + p_3 + p_4}{4}. \quad (12)$$

Second, the pressure can be estimated as the pressure from the origin microphone,¹⁴

$$p \approx p_1. \quad (13)$$

Third, the pressure can be estimated using a weighted average of the pressures favoring the origin microphone,

$$p \approx \frac{1}{3} \left(\frac{p_1 + p_2}{2} + \frac{p_1 + p_3}{2} + \frac{p_1 + p_4}{2} \right). \quad (14)$$

This weighted pressure estimate has been suggested as an alternative to the ordinary pressure average in Eq. (12) because it estimates the pressure at the point $(h/3, h/3, h/3)$, which is closer than the point $(h/2, h/2, h/2)$ of the Eq. (12) average to $(h, 0, 0)$, $(0, h, 0)$, and $(0, 0, h)$, where the velocity is estimated when Eq. (3) is used.¹³

The Taylor expansion for collocating velocity estimates, as described previously, leads to a new method for estimating pressure. A Taylor expansion of the measured pressures can be used to estimate the pressure at (h, h, h) , collocated with the velocity estimates. This can be done by the same process as was used for the velocity in Eqs. (4)–(6), substituting pressure for x -direction velocity in the following manner:

$$p(h, h, h) \approx p(h, 0, 0) + h \frac{\partial p}{\partial y} \Big|_{(h,0,0)} + h \frac{\partial p}{\partial z} \Big|_{(h,0,0)}, \quad (15)$$

where the derivatives are estimated using the first-order finite differences

$$\begin{aligned} \frac{\partial p}{\partial y} \Big|_{(h,0,0)} &\approx \frac{p(h, h, 0) - p(h, 0, 0)}{h}, \\ \frac{\partial p}{\partial z} \Big|_{(h,0,0)} &\approx \frac{p(h, 0, h) - p(h, 0, 0)}{h}. \end{aligned} \quad (16)$$

This results in

$$p(h, h, h) \approx p(h, h, 0) + p(h, 0, h) - p(h, 0, 0). \quad (17)$$

If each of the three pressure terms is given as an average between pairs of microphones, for example, $p(h, h, 0) \approx (p_2 + p_3)/2$ then

$$p(h, h, h) \approx \frac{p_2 + p_3 + p_4 - p_1}{2}. \quad (18)$$

Note that the same pressure estimate results if the Taylor expansion is used starting from the y -direction or z -direction analogous to the velocity estimates in Eqs. (10) and (11), or if the expansion is carried out relative to the origin microphone. Although the Taylor expansion for velocity was described previously by Locey,¹⁸ the method of pressure estimation in Eq. (18) is unique to this work.

The final method of estimating pressure is to use a different pressure estimate for each of the three orthogonal directions. The intensity in each orthogonal direction is calculated using the average of only the pressures measured by the two microphones along that direction. For example, the x -direction intensity is calculated as

$$\begin{aligned} I_x &= \frac{1}{2} \text{Re} \{ p_x v_x^* \} \\ &= \frac{1}{2} \text{Re} \left\{ \left(\frac{p_1 + p_2}{2} \right) v_x^* \right\} \end{aligned} \quad (19)$$

and the total intensity vector can then be obtained from the three orthogonal intensity estimates. When the pressure is estimated this way in conjunction with the three points velocity estimate the orthogonal probe is essentially being used as three one-dimensional probes, such as the probe used by Vandenhout *et al.*¹⁹ However, it was found that when using the three points velocity estimate this pressure estimate is equivalent to using the pressure estimate in Eq. (13). This is a non-obvious result, and is proven mathematically in the Appendix.

The pressure estimate method in Eq. (19) could also be used with the Taylor expansion velocity estimate, however, the purpose of using the Taylor expansion is then negated as there are then three non-collocated pressure estimates. Although the velocity estimate is then at point (h, h, h) , the pressure estimates are at $(h, 0, 0)$, $(0, h, 0)$, and $(0, 0, h)$. As this pressure estimate method is not useful with the one velocity estimate and redundant with the other velocity estimate, it is not considered further in this paper.

C. Summary of estimation methods

The two ways of estimating the particle velocity combined with the four ways of estimating the pressure lead to eight ways of estimating intensity with an orthogonal probe considered here. These processing methods can either be used with microphones mounted in a sphere or not, resulting in 16 total probe types. This paper investigates the errors of each of these methods in measuring the magnitude and the angle of active intensity for orthogonal probes.

Table I summarizes all intensity processing types and identifies each by an abbreviation. If the probe type has the microphones mounted on a sphere, the abbreviation “S/” is used. In estimating the pressure, “A” signifies that the average

TABLE I. Summary and abbreviations of considered methods used to estimate intensity with the orthogonal probe.

Abbreviation	Scattering	Pressure estimate	Velocity estimate
A.3	None	$p = \frac{p_1 + p_2 + p_3 + p_4}{4}$	Three points
I.3	None	$p = p_1$	Three points
W.3	None	$p = \frac{1}{3} \left(\frac{p_1 + p_2}{2} + \frac{p_1 + p_3}{2} + \frac{p_1 + p_4}{2} \right)$	Three points
T.3	None	$p = \frac{p_2 + p_3 + p_4 - p_1}{2}$	Three points
A.T	None	$p = \frac{p_1 + p_2 + p_3 + p_4}{4}$	Taylor approximation
I.T	None	$p = p_1$	Taylor approximation
W.T	None	$p = \frac{1}{3} \left(\frac{p_1 + p_2}{2} + \frac{p_1 + p_3}{2} + \frac{p_1 + p_4}{2} \right)$	Taylor approximation
T.T	None	$p = \frac{p_2 + p_3 + p_4 - p_1}{2}$	Taylor approximation
S/A.3	Spherical	$p = \frac{p_1 + p_2 + p_3 + p_4}{4}$	Three points
S/I.3	Spherical	$p = p_1$	Three points
S/W.3	Spherical	$p = \frac{1}{3} \left(\frac{p_1 + p_2}{2} + \frac{p_1 + p_3}{2} + \frac{p_1 + p_4}{2} \right)$	Three points
S/T.3	Spherical	$p = \frac{p_2 + p_3 + p_4 - p_1}{2}$	Three points
S/A.T	Spherical	$p = \frac{p_1 + p_2 + p_3 + p_4}{4}$	Taylor approximation
S/I.T	Spherical	$p = p_1$	Taylor approximation
S/W.T	Spherical	$p = \frac{1}{3} \left(\frac{p_1 + p_2}{2} + \frac{p_1 + p_3}{2} + \frac{p_1 + p_4}{2} \right)$	Taylor approximation
S/T.T	Spherical	$p = \frac{p_2 + p_3 + p_4 - p_1}{2}$	Taylor approximation

of the four microphones is used as in Eq. (12), “1” that the pressure from one microphone is used as in Eq. (13), “W” that the weighted four-microphone average is used as in Eq. (14), and “T” that the Taylor approximation is used as in Eq. (18). A period is followed by the abbreviation for the velocity estimate where “3” is for the typical three points estimate as given in Eq. (3) and “T” for the Taylor approximation as given in Eqs. (6), (10), and (11).

III. CROSS-SPECTRAL FORMULATIONS

Cross-spectral formulas allow the intensity to be calculated in the frequency domain using the cross spectra from the different time signals measured by the microphones. The one-sided cross-spectral density for a zero-mean process is defined as

$$G_{mn}(\omega) = C_{mn}(\omega) + jQ_{mn}(\omega) = \lim_{T \rightarrow \infty} \frac{2}{T} E[P_m^*(\omega, T)P_n(\omega, T)] \quad (20)$$

for $\omega \geq 0$, where P_m and P_n are the Fourier transforms of the pressures from the m th and n th microphones, respectively, over time T . The expectation operator is denoted by $E[\cdot]$. The real part of the cross-spectral density G is defined as the cospectral density, C , and the imaginary part as the quad-spectral density, Q . Some of these equations have been presented by Pascal and Li,¹⁴ but all are given here for completeness. The formulas given are for probes with microphones freely suspended in space; the variable h must be multiplied by 3/2 if instead the microphones are mounted in a sphere. Although not explicitly written in the following

equations for brevity, all cross-spectral densities (and hence intensities) are functions of frequency. The equation for the probe type abbreviated “1.3” is

$$\mathbf{I}_{1.3} = \begin{cases} I_x \approx \frac{Q_{21}}{2h\rho\omega} \\ I_y \approx \frac{Q_{31}}{2h\rho\omega} \\ I_z \approx \frac{Q_{41}}{2h\rho\omega}; \end{cases} \quad (21)$$

probe type “A.3,”

$$\mathbf{I}_{A.3} = \begin{cases} I_x \approx \frac{1}{8h\rho\omega} (2Q_{21} + Q_{31} + Q_{41} - Q_{32} - Q_{42}) \\ I_y \approx \frac{1}{8h\rho\omega} (Q_{21} + 2Q_{31} + Q_{41} + Q_{32} - Q_{43}) \\ I_z \approx \frac{1}{8h\rho\omega} (Q_{21} + Q_{31} + 2Q_{41} + Q_{42} + Q_{43}); \end{cases} \quad (22)$$

probe type “W.3,”

$$\mathbf{I}_{W.3} = \begin{cases} I_x \approx \frac{1}{12h\rho\omega} (4Q_{21} + Q_{31} + Q_{41} - Q_{32} - Q_{42}) \\ I_y \approx \frac{1}{12h\rho\omega} (Q_{21} + 4Q_{31} + Q_{41} + Q_{32} - Q_{43}) \\ I_z \approx \frac{1}{12h\rho\omega} (Q_{21} + Q_{31} + 4Q_{41} + Q_{42} + Q_{43}); \end{cases} \quad (23)$$

probe type “T.3,”

$$\mathbf{I}_{T,3} = \begin{cases} I_x \approx \frac{1}{4h\rho\omega} (Q_{31} + Q_{41} - Q_{32} - Q_{42}) \\ I_y \approx \frac{1}{4h\rho\omega} (Q_{21} + Q_{41} + Q_{32} - Q_{43}) \\ I_z \approx \frac{1}{4h\rho\omega} (Q_{21} + Q_{31} + Q_{42} + Q_{43}); \end{cases} \quad (24)$$

and probe type “1. T,”

$$\mathbf{I}_{1.T} = \begin{cases} I_x \approx A_1 [A_2(Q_{31} - Q_{21}) + A_3(Q_{41} - Q_{21}) - \sqrt{2}Q_{21}] \\ I_y \approx A_1 [A_4(Q_{31} - Q_{21}) + A_5(Q_{41} - Q_{31}) - \sqrt{2}Q_{31}] \\ I_z \approx A_1 [A_6(Q_{41} - Q_{21}) + A_7(Q_{41} - Q_{31}) - \sqrt{2}Q_{41}], \end{cases} \quad (25)$$

with

$$\begin{aligned} A_1 &= \frac{1}{2\sqrt{2}h\rho\omega}, \\ A_2 &= \frac{\cos(\theta_{xy})}{\cos\left(\frac{3\pi}{4} - \theta_{xy}\right)}, \\ A_3 &= \frac{\cos(\theta_{xz})}{\cos\left(\frac{3\pi}{4} - \theta_{xz}\right)}, \\ A_4 &= \frac{\sin(\theta_{xy})}{\cos\left(\frac{3\pi}{4} - \theta_{xy}\right)}, \\ A_5 &= \frac{\cos(\theta_{yz})}{\cos\left(\frac{3\pi}{4} - \theta_{yz}\right)}, \\ A_6 &= \frac{\sin(\theta_{xz})}{\cos\left(\frac{3\pi}{4} - \theta_{xz}\right)}, \\ A_7 &= \frac{\sin(\theta_{yz})}{\cos\left(\frac{3\pi}{4} - \theta_{yz}\right)}, \end{aligned} \quad (26)$$

where

$$\begin{aligned} \theta_{xy} &= \tan^{-1} \sqrt{\frac{G_{33} + G_{11} - 2C_{13}}{G_{22} + G_{11} - 2C_{12}}}, \\ \theta_{xz} &= \tan^{-1} \sqrt{\frac{G_{44} + G_{11} - 2C_{14}}{G_{22} + G_{11} - 2C_{12}}}, \\ \theta_{yz} &= \tan^{-1} \sqrt{\frac{G_{44} + G_{11} - 2C_{14}}{G_{33} + G_{11} - 2C_{13}}}. \end{aligned} \quad (27)$$

However, these angles might need to be multiplied by -1 depending on the phase relations between the different velocity components as shown by Eq. (8) for θ_{xy} . But for this step to be performed in terms of cross-spectra, the phase between intensity components is compared instead of between velocity components. This assumes that the pressure estimates of the intensities are equivalent, which they are not; however, the assumption serves as a satisfactory approximation. Mathematically, this is given by

$$\begin{aligned} \theta_{xy} &= -\theta_{xy} \quad \text{if } \frac{\pi}{2} \leq \left| \arg\left(\frac{Q_{21}}{Q_{31}}\right) \right| \leq \frac{3\pi}{2}, \\ \theta_{xz} &= -\theta_{xz} \quad \text{if } \frac{\pi}{2} \leq \left| \arg\left(\frac{Q_{21}}{Q_{41}}\right) \right| \leq \frac{3\pi}{2}, \\ \theta_{yz} &= -\theta_{yz} \quad \text{if } \frac{\pi}{2} \leq \left| \arg\left(\frac{Q_{31}}{Q_{41}}\right) \right| \leq \frac{3\pi}{2}. \end{aligned} \quad (28)$$

Probe type “A.T,”

$$\mathbf{I}_{A.T} = \begin{cases} I_x \approx A_8(A_2A_9 + A_3A_{10} - \sqrt{2}A_{11}) \\ I_y \approx A_8(A_4A_9 + A_5A_{12} - \sqrt{2}A_{13}) \\ I_z \approx A_8(A_6A_{10} + A_7A_{12} - \sqrt{2}A_{14}) \end{cases} \quad (29)$$

with

$$\begin{aligned} A_8 &= \frac{1}{8\sqrt{2}h\rho\omega}, \\ A_9 &= -Q_{21} + Q_{31} + 2Q_{32} + Q_{42} - Q_{43}, \\ A_{10} &= -Q_{21} + Q_{41} + Q_{32} + 2Q_{42} + Q_{43}, \\ A_{11} &= 2Q_{21} + Q_{31} + Q_{41} - Q_{32} - Q_{42}, \\ A_{12} &= -Q_{31} + Q_{41} - Q_{32} + Q_{42} + 2Q_{43}, \\ A_{13} &= Q_{21} + 2Q_{31} + Q_{41} + Q_{32} - Q_{43}, \\ A_{14} &= Q_{21} + Q_{31} + 2Q_{41} + Q_{42} + Q_{43}. \end{aligned} \quad (30)$$

probe type “W.T,”

$$\mathbf{I}_{W.T} = \begin{cases} I_x \approx A_{15}(A_2A_{16} + A_3A_{17} - \sqrt{2}A_{18}) \\ I_y \approx A_{15}(A_4A_{16} + A_5A_{19} - \sqrt{2}A_{20}) \\ I_z \approx A_{15}(A_6A_{17} + A_7A_{19} - \sqrt{2}A_{21}) \end{cases} \quad (31)$$

with

$$\begin{aligned} A_{15} &= \frac{1}{12\sqrt{2}h\rho\omega}, \\ A_{16} &= 3Q_{21} + 3Q_{31} + 2Q_{32} + Q_{42} - Q_{43}, \\ A_{17} &= 3Q_{21} + 3Q_{41} + Q_{32} + 2Q_{42} + Q_{43}, \\ A_{18} &= 4Q_{21} + Q_{31} + Q_{41} - Q_{32} - Q_{42}, \\ A_{19} &= -3Q_{31} + 3Q_{41} - Q_{32} + Q_{42} + 2Q_{43}, \\ A_{20} &= Q_{21} + 4Q_{31} + Q_{41} + Q_{32} - Q_{43}, \\ A_{21} &= Q_{21} + Q_{31} + 4Q_{41} + Q_{42} + Q_{43}; \end{aligned} \quad (32)$$

and probe type “T.T,”

$$\mathbf{I}_{T.T} = \begin{cases} I_x \approx A_{22}(A_2A_{23} + A_3A_{24} - \sqrt{2}A_{25}) \\ I_y \approx A_{22}(A_4A_{23} + A_5A_{26} - \sqrt{2}A_{27}) \\ I_z \approx A_{22}(A_6A_{24} + A_7A_{26} - \sqrt{2}A_{28}) \end{cases} \quad (33)$$

with

$$\begin{aligned} A_{22} &= \frac{1}{4\sqrt{2}h\rho\omega}, \\ A_{23} &= Q_{21} - Q_{31} + 2Q_{32} + Q_{42} - Q_{43}, \\ A_{24} &= Q_{21} - Q_{41} + Q_{32} + 2Q_{42} + Q_{43}, \\ A_{25} &= Q_{31} + Q_{41} - Q_{32} - Q_{42}, \\ A_{26} &= Q_{31} - Q_{41} - Q_{32} + Q_{42} + 2Q_{43}, \\ A_{27} &= Q_{21} + Q_{41} + Q_{32} - Q_{43}, \\ A_{28} &= Q_{21} + Q_{31} + Q_{42} + Q_{43}. \end{aligned} \quad (34)$$

IV. COMPARISON MODEL

An indication of the relative merit of any one implementation can be obtained by examining the errors of a probe consisting of perfect point sensors simulated in a plane-wave field. In order to directly compare the orthogonal probe types, a suitable dimensionless variable is needed. The variable ka is used, where k is the wavenumber and a is the radius of the sphere for spherical probes, or, in the case of freely suspended probes, it is the radius of an imaginary sphere that is circumscribed for the four microphone points. This radius relates to the microphone separation distance $2h$ through the relation $h = (\sqrt{6}/3)a$. However, for direct comparison the spherical probe is compared to a freely suspended probe that is $3/2$ times larger. This is done because, as described previously, at low frequencies the effective separation distance of microphones mounted in a sphere is $3/2$ times greater than for those not mounted in a sphere. That is, the error at any given frequency ka for the freely suspended probe is compared to the error at $\frac{3}{2}ka$ for the spherical probe. This approach was used by both Elko¹⁷ and Parkins *et al.*¹²

The time-harmonic complex pressure at any microphone on the surface of a rigid sphere of radius a in a plane-wave field consists of incident and scattered pressure. Taking the center of the sphere as the origin, the total pressure can be given (using the $e^{j\omega t}$ time convention) by the series solution²²

$$p_i = \frac{P_0}{j(ka)^2} \sum_{n=0}^{\infty} \frac{j^n (2n+1) P_n(\cos \theta)}{h_n^{(2)'}(ka)} \quad (35)$$

where p_i is the pressure at the i th microphone, P_0 the amplitude of the plane wave, $P_n(\cos \theta)$ the Legendre polynomial of order n , θ the angle between the incident plane wave and the i th microphone, and $h_n^{(2)'}$ the derivative of the spherical Hankel function of the second type of order n . When scattering is not accounted for, the pressure at the i th microphone on the surface of an imaginary sphere of radius a is just the incident pressure given by

$$p_i = P_0 e^{jka \cos \theta}. \quad (36)$$

Higher frequencies generally require more terms in the expansion to adequately calculate the scattering. Figure 4 shows the percent error of the pressure as a fraction of the actual pressure as more terms in the series are included for a plane wave directly incident on a microphone location ($\theta=0$). Other angles of incidence yield similar results. The “actual” pressure is calculated using a very large number of terms in the series solution. Results up to $ka = \pi/2$ for freely suspended designs (corresponding to the sphere diameter being a half-wavelength) and $\frac{3}{2}ka = \pi/2$ for spherical designs are considered in this paper, and so 25 terms are shown to be more than sufficient in the scattering calculation. For the probe types with microphones not mounted in a sphere scattering was neglected as it would vary dependent on the size and configuration of the microphones and holders.

The measurement error of any probe design is dependent on the angle of incidence of the travelling plane wave in relation to the probe. Certain angles of incidence correspond

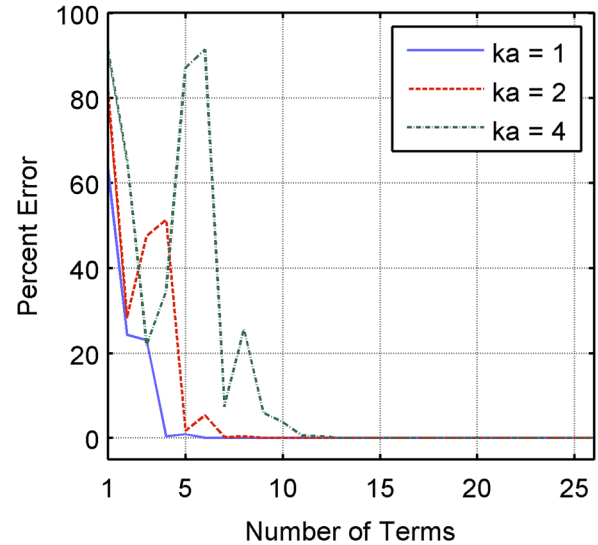


FIG. 4. (Color online) Magnitude of percent error in the scattered pressure calculation as a function of the number of terms used in the infinite expansion.

to underestimation of intensity, whereas others correspond to overestimation. This angle-dependent error is illustrated in Fig. 5(a), which shows the intensity magnitude error of the orthogonal probe type “1.3” as an example. The figure shows the error (in dB) of the probe estimate relative to the actual intensity magnitude when the probe is exposed to plane waves at different angles of incidence for $ka = \pi/32$ (on left) and $ka = \pi/2$ (on right). For example, if the monochromatic plane wave is incident on the top of the probe, it is expected that the probe will underestimate the intensity magnitude by ~ 0.009 dB at $ka = \pi/32$ and overestimate by about 2.7 dB at $ka = \pi/2$.

Three metrics are used in this paper for probe type comparison. First, maximum error, corresponding to the worst possible probe orientation, is plotted to show the extreme errors associated with each implementation. Both underestimation and overestimation are undesired so the maximum error corresponds to either. For example, this metric is calculated to be 0.009 dB for Fig. 5(a), corresponding to the error seen at four different angles of incidence (one on the back side is not seen). Second, a root mean square (rms) error metric is used. This metric is representative of the magnitude error expected if the probe were to be randomly oriented in a sound field and is calculated as the rms average of the decibel errors. Using Fig. 5(b) as an example, the rms error is 1.

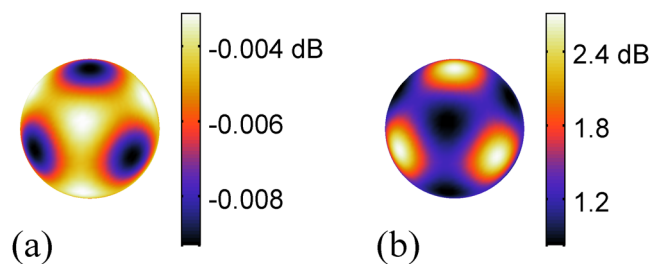


FIG. 5. (Color online) Intensity magnitude errors as a function of incidence angle for probe type “1.3” at (a) $ka = \pi/32$ and (b) $ka = \pi/2$.

6 dB. The third metric is the difference between the maximum and minimum intensity magnitude errors. This metric must be calculated before taking the absolute value of the errors; in the example of Fig. 5(b), it is seen to be ~ 1.9 dB. The intensity magnitude error spread is a useful metric because it indicates how well the probe type can be calibrated for magnitude. Better calibration can be achieved if the spread is smaller.

The simulation calculated intensity error at angles of incidence that were equally spaced using the angular spherical coordinates θ and ϕ . Figure 6 shows the simulated incidence angles as the points of intersection of the latitude and longitude lines. The error, in dB, for intensity magnitude, at an incidence angle (θ_i, ϕ_j) was calculated using

$$\mathbf{I}_{mag\ err}(\theta_i, \phi_j) = 10 \log \frac{\|\mathbf{I}_{est}(\theta_i, \phi_j)\|}{\|\mathbf{I}_{exact}\|}, \quad (37)$$

where the estimated intensity magnitude $\|\mathbf{I}_{est}(\theta_i, \phi_j)\|$ is specific to incidence angle (θ_i, ϕ_j) , whereas the actual intensity magnitude $\|\mathbf{I}_{exact}\|$ is not. The intensity direction error was calculated in degrees using

$$\mathbf{I}_{dir\ err}(\theta_i, \phi_j) = \frac{180}{\pi} \cos^{-1} \left(\frac{\mathbf{I}_{est}(\theta_i, \phi_j) \cdot \mathbf{I}_{exact}}{\|\mathbf{I}_{est}(\theta_i, \phi_j)\| \|\mathbf{I}_{exact}\|} \right), \quad (38)$$

where the angle is calculated by dividing the dot product by the magnitude values.

However, this setup results in a greater number of angles of incidence evaluated near the poles as can be seen in Fig. 6, so an rms average error value would favor these areas of incidence angle. The rms average error metric was therefore calculated by multiplying the squared error values by an appropriate weighting function, w_i ,

$$I_{err, RMS} = \sqrt{\frac{\sum_{j=1}^m \sum_{i=1}^n w_i I_{err}(\theta_i, \phi_j)^2}{m \sum_{i=1}^n w_i}}, \quad (39)$$

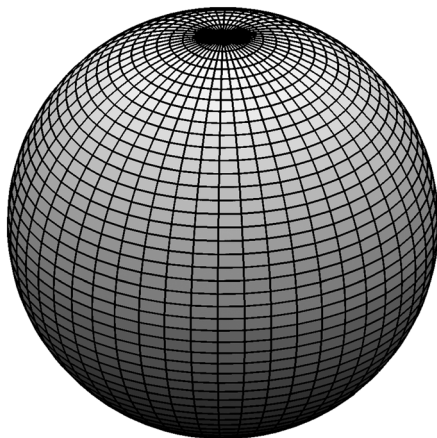


FIG. 6. Angles of incidence considered shown as the intersection points of lines of latitude and longitude.

where I_{err} is either $I_{mag\ err}$ or $I_{dir\ err}$ with $n = \theta_{step}/\pi + 1$ and $m = \phi_{step}/\pi + 1$. This is similar to the process used by Leishman *et al.*²³ and Monson *et al.*,²⁴ in which equal-angle, three-dimensional directivity measurements were area-weighted.

The weighting function converted the results from the equal-angle spacing used in the simulation to equal-area spacing, more appropriate in calculating the rms average error as it does not favor the poles. The weighting function is given by

$$w_i = \cos \theta_i - \cos \theta_{i+1}, \quad (40)$$

with

$$\theta_i = \begin{cases} 0, & i = 1 \\ \theta_{step}(i-2) + \frac{\theta_{step}}{2}, & i = 2, 3, \dots, n-1 \\ \pi, & i = n. \end{cases} \quad (41)$$

A suitable step size was found to be $\theta_{step} = \phi_{step} = \pi/50$. The step size needed to be suitably small to achieve a fine enough mesh of sample points, but also needed to be chosen carefully because certain step sizes (such as $\theta_{step} = \phi_{step} = s\pi/4$ for $s = 1, 2, 3, \dots$) led to some very large errors when using the Taylor approximation. Using these step sizes resulted in one specific sample point that had very large errors due to the geometric properties of the probe and the Taylor approximation processing method for calculating intensity. Therefore, using an appropriate step size meant avoiding such particular angles of incidence from being sampled in order to avoid the large errors and obtain more meaningful results. These large errors were seen to affect the maximum error metric, but not the rms average error metric as the one large-error angle of incidence was ‘‘averaged out’’ with all the other angles of incidence. However, no large-error problems were seen to occur for any metric for the step size $\pi/50$.

V. RESULTS

Four pressure estimates multiplied by two velocity estimates (one using and one not using the Taylor expansion) results in eight processing methods. These processing methods can be used with probes mounted in a sphere or not, making 16 total probe types whose errors are plotted.

A. Intensity magnitude errors

Figure 7 shows the rms average and maximum intensity magnitude errors of the probe types not mounted in a sphere. In all of the following figures, graphs (a) and (c) correspond to the particle velocity being estimated by a three-point velocity estimate, whereas graphs (b) and (d) correspond to the estimate using the first-order Taylor approximation. The different pressure estimates are given as the different lines in the plots. The top two graphs, (a) and (b), show rms average errors, whereas the bottom two, (c) and (d), show maximum errors.

Figures 7(a) and 7(c) show that when the three points velocity estimate is used the lowest rms average and maximum

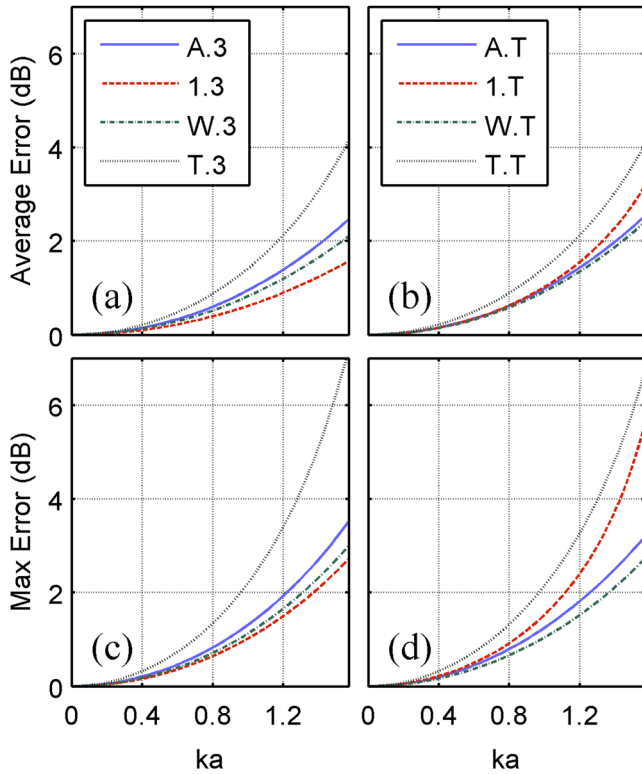


FIG. 7. (Color online) Root mean square average intensity magnitude errors for freely suspended designs using either the three points (a) or Taylor approximation (b) velocity estimate and corresponding maximum errors (c) and (d).

errors result from using the pressure of the origin microphone (“1.3”). Conversely, when the Taylor approximation is used the origin microphone pressure gives the most error (“1.T”). Comparing left- and right-hand graphs, lower errors are generally seen when a three-point velocity estimate is used instead of the Taylor approximation. Overall, the best processing method for calculating intensity magnitude when not using a sphere is to use the three-point velocity estimate and the origin microphone for the pressure estimate (“1.3”).

Results for the probe types with microphones mounted in a sphere are shown in Fig. 8 and show similar results. Again the best combination is to use the origin microphone pressure with a three-point velocity estimate (“S/1.3”). Comparing Figs. 7 and 8 reveals that overall the spherical designs perform slightly better than their freely suspended counterparts with scaled microphone spacing. The probe type that exhibits the least rms average and max error in calculating intensity magnitude is shown to result from using the origin pressure microphone without the Taylor approximation with the microphones embedded on a sphere (“S/1.3”).

B. Intensity direction errors

The errors in estimating the intensity direction are important because often three-dimensional intensity measurements are used for sound source localization. In these situations the direction errors tend to be unacceptable at an upper-frequency limit that is lower than that for the magnitude errors. The direction errors are plotted here in degrees, referring to the angle between the three-dimensional actual

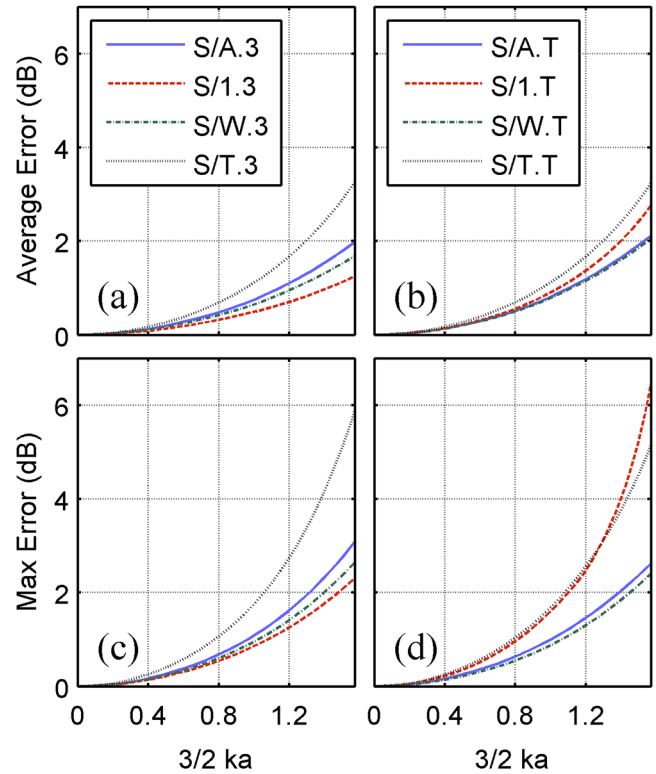


FIG. 8. (Color online) Root mean square average intensity magnitude errors for spherical designs using either the three points (a) or Taylor approximation (b) velocity estimate and corresponding maximum errors (c) and (d).

vector intensity and the vector intensity estimated by the probe. The errors for the probe types not mounted in a sphere are shown in Fig. 9.

The left-hand graphs in Fig. 9 show that probe type “T.3” has considerably more direction error than the others using the three-point velocity estimate. But when the Taylor expansion pressure is combined with the Taylor expansion velocity (“T.T”), the lowest intensity direction error is obtained. Comparing left- to right-hand graphs shows that, in contrast to the intensity magnitude results, the Taylor approximation probe types outperform the three-point velocity types for intensity direction.

The direction errors for probe types mounted in a sphere are shown next in Fig. 10. The results are similar to those for freely suspended probes: Using the Taylor expansion pressure is useful with the Taylor expansion velocity (“S/T.T”), but not with the three points velocity (“S/T.3”). The Taylor expansion velocity exhibits less error than the three-point velocity. Comparing Figs. 9 and 10, the spherical designs all exhibit equal or less error than the corresponding freely suspended designs. Overall, the lowest-error method for estimating intensity direction is thus to use a spherical probe with the Taylor expansion pressure and velocity estimates (“S/T.T”). A summary of probe types that had the lowest errors is shown in Table II.

C. Effect of using Taylor approximation

The effect of using the Taylor approximation for the velocity estimate instead of the three-point estimate can be analyzed by looking at the difference in error between any

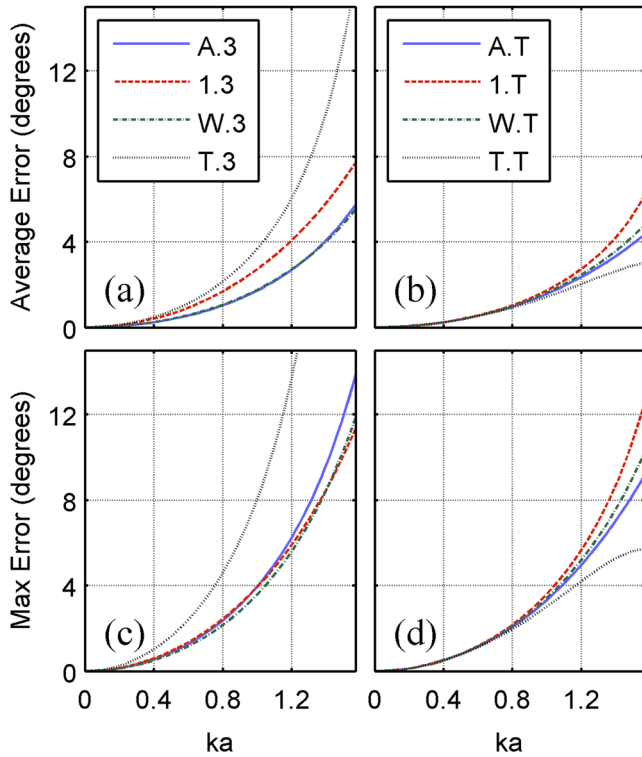


FIG. 9. (Color online) Root mean square average intensity direction errors for freely suspended designs using either the three points (a) or Taylor approximation (b) velocity estimate and corresponding maximum errors (c) and (d).

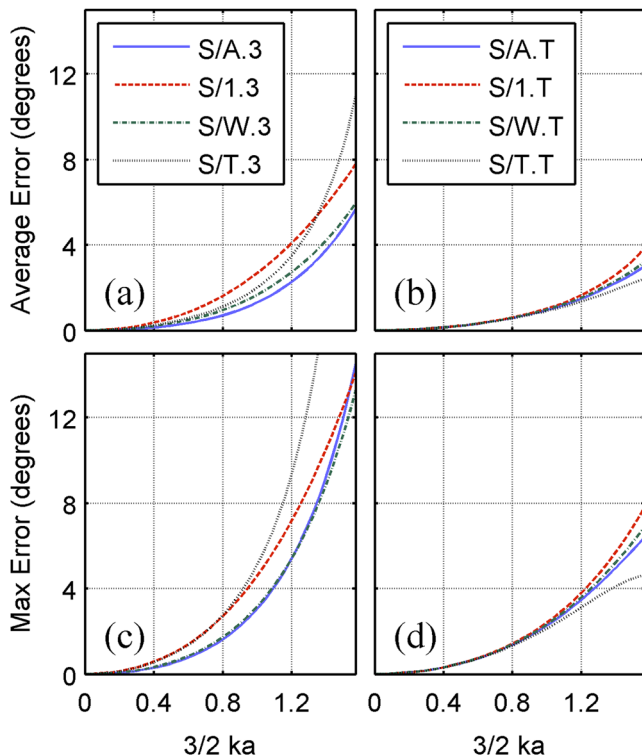


FIG. 10. (Color online) Root mean square average intensity direction errors for spherical designs using either the three points (a) or Taylor approximation (b) velocity estimate and corresponding maximum errors (c) and (d).

TABLE II. Probe type with least error for each probe design and quantity of interest.

Quantity	Non-sphere design	Sphere design	Overall
Intensity magnitude	1.3	S/1.3	S/1.3
Intensity direction	T.T	S/T.T	S/T.T

Taylor approximation probe type and its corresponding three-point probe type. Table III shows these results for rms average intensity magnitude error (labeled “Magnitude”), intensity magnitude error spread (labeled “Magnitude spread”), and rms average intensity direction error (labeled “Direction”) at the highest frequency considered. Examining the errors only at the highest frequency considered is sufficient as all error curves have been seen to be monotonically increasing with generally no one curve crossing over any other curve; that is, the probe types generally remain in the same order of highest to lowest error independent of frequency. A positive value indicates that using the Taylor approximation led to more error than using the three-point estimate. For example the first row of the Table III shows that, when using the normal average for the pressure estimate, the Taylor expansion velocity (“A.T”) gives 0.07 dB more rms average error in estimating intensity magnitude than using the three points velocity (“A.3”) at that frequency.

Table III indicates that using the Taylor approximation is beneficial by up to a few degrees when estimating intensity direction, but not beneficial for intensity magnitude (except for the two Taylor expansion pressure probe types). In most cases the magnitude error spread is made worse by the Taylor approximation.

D. Effect of mounting microphones in sphere

A similar analysis can be performed to compare spherical and freely suspended designs. Table IV shows the error difference between spherical and freely suspended designs at the highest frequency considered. A positive value indicates that the spherical design resulted in more error than its freely suspended counterpart. Mounting the microphones in a sphere is seen to always result in less error for intensity magnitude and for all cases but “1.3” and “W.3” for intensity direction. However, for magnitude spread, half of the probe types are made worse by the spherical scattering.

TABLE III. Error difference between Taylor approximation probe types and three points probe types at the highest frequency considered.

Probe type	Magnitude (dB)	Magnitude spread (dB)	Direction (deg)
A.T–A.3	0.07	0.92	–1.40
1.T–1.3	1.62	2.46	–1.49
W.T–W.3	0.31	–0.27	–0.72
T.T–T.3	–0.08	3.15	–13.45
S/A.T–S/A.3	0.13	–1.00	–2.67
S/1.T–S/1.3	1.52	3.10	–3.90
S/W.–S/W.3	0.37	–1.84	–2.74
S/T.T–S/T.3	–0.03	1.19	–8.51

TABLE IV. Error difference between spherical and freely suspended probe designs at the highest frequency considered.

Probe type	Magnitude (dB)	Magnitude spread (dB)	Direction (deg)
S/A.3–A.3	−0.49	0.66	−0.09
S/1.3–1.3	−0.33	0.69	0.05
S/W.3–W.3	−0.42	0.75	0.42
S/T.3–T.3	−0.89	−0.29	−5.54
S/A.T–A.T	−0.42	−1.25	−1.36
S/1.T–1.T	−0.43	1.32	−2.36
S/W.T–W.T	−0.36	−0.82	−1.61
S/T.T–T.T	−0.84	−2.25	−0.60

VI. CONCLUSIONS

General trends from the simulations show that using the Taylor approximation for the particle velocity estimate gives better probe accuracy than the three-point estimate for intensity direction, but worse accuracy for intensity magnitude. Also seen is that spherical designs generally exhibit lower error than their freely suspended counterparts. The idea of using a weighted average of the microphones to put the pressure estimate at a point nearer to the three points, where the three-point velocity is estimated (“W.3” and “S/W.3”) is shown to give marginally better results than those of the normal pressure average (“A.3” and “S/A.3”). The idea of using Taylor expansions to put the pressure and velocity estimates at the same point in space is shown to be useful in that it gives the lowest errors for intensity direction, although it is not preferable for intensity magnitude.

If the quantity of interest is intensity magnitude, the best results come from probe type “S/1.3”: A spherical design using the origin microphone for the pressure estimate and the three-point velocity estimate. Alternatively, if intensity direction is desired, probe type “S/T.T” gives lowest error: A spherical design with pressure and velocity estimated using Taylor approximations. This study suggests then that in plane-wave fields, the lowest errors are generally attained when the microphones of the orthogonal probe are mounted on the surface of a sphere and if the data recorded from the microphones are processed one way for intensity magnitude and another for intensity direction. A prototype of this type of probe is described by Locey¹⁸ and Oldham.²⁵

The results of this study are useful in showing the relative merit of each processing method; however, most all of the rms average intensity magnitude errors were within ~ 1 – 2 dB of each other at the highest frequency considered, a fairly negligible amount. For intensity direction, the best probe types were up to ~ 12 degrees better than the worst, which is likely more significant than the intensity magnitude error spread. However, because the results presented in this paper are for ideal sensors in plane-wave fields, results may differ for reactive fields or if effects such as noise and/or sensor mismatch are included.

For the intensity magnitude results, average error curves similar to those shown in this paper could be advantageously used as calibration curves for any particular processing method, effectively decreasing the maximum error at any frequency by the amount of average error at that frequency.

However, instead of using the rms average error, the signed average error should be used for the calibration. A similar process would not work for intensity direction, as the incidence angle is a two-dimensional quantity, whereas the intensity direction error is a one-dimensional angle. Further work could examine the direction errors in terms of the two components θ and ϕ , allowing for the development of intensity direction calibration curves.

ACKNOWLEDGMENTS

This work was supported in part by the NASA Stennis Space Center Small Business Innovative Research program through a subcontract from Blue Ridge Research and Consulting.

APPENDIX: MATHEMATICAL EQUIVALENCE OF PROBE TYPES “3 1D” AND “1”

The expression for the vector active intensity if the orthogonal probe is implemented as three one-dimensional probes (“3 1D”) is given using complex notation by

$$\mathbf{I} = \begin{cases} I_x \approx \frac{1}{2} \operatorname{Re} \left\{ \frac{p_1 + p_2}{2} v_x^* \right\} \\ I_y \approx \frac{1}{2} \operatorname{Re} \left\{ \frac{p_1 + p_3}{2} v_y^* \right\} \\ I_z \approx \frac{1}{2} \operatorname{Re} \left\{ \frac{p_1 + p_4}{2} v_z^* \right\}, \end{cases} \quad (\text{A1})$$

where p_1 is the pressure from the origin microphone and $p_2, p_3,$ and p_4 are the pressures from the microphones on the x -, y -, and z -axes; particle velocities in the three orthogonal directions are given by $v_x, v_y,$ and v_z ; the complex conjugate is denoted by an asterisk, and the real part is denoted by “Re.” Using the time-harmonic linear Euler’s equation

$$\mathbf{v} = \frac{j \nabla p}{\rho \omega}, \quad (\text{A2})$$

with ρ being the fluid density and ω the angular frequency in conjunction with a first-order finite-difference approximation of the pressure gradient, the following is obtained and then simplified as follows:

$$\mathbf{I} = \begin{cases} I_x \approx \frac{1}{2} \operatorname{Re} \left\{ \frac{p_1 + p_2}{2} \left(\frac{j(p_2 - p_1)}{2h\rho\omega} \right)^* \right\} \\ I_y \approx \frac{1}{2} \operatorname{Re} \left\{ \frac{p_1 + p_3}{2} \left(\frac{j(p_3 - p_1)}{2h\rho\omega} \right)^* \right\} \\ I_z \approx \frac{1}{2} \operatorname{Re} \left\{ \frac{p_1 + p_4}{2} \left(\frac{j(p_4 - p_1)}{2h\rho\omega} \right)^* \right\} \end{cases} \\ = \begin{cases} \frac{1}{2} \operatorname{Re} \left\{ \frac{p_1 + p_2 - j(p_2^* - p_1^*)}{2h\rho\omega} \right\} \\ \frac{1}{2} \operatorname{Re} \left\{ \frac{p_1 + p_3 - j(p_3^* - p_1^*)}{2h\rho\omega} \right\} \\ \frac{1}{2} \operatorname{Re} \left\{ \frac{p_1 + p_4 - j(p_4^* - p_1^*)}{2h\rho\omega} \right\} \end{cases}$$

$$\begin{aligned}
&= \begin{cases} \frac{1}{8h\rho\omega} \text{Im}\{(p_1 + p_2)(p_2^* - p_1^*)\} \\ \frac{1}{8h\rho\omega} \text{Im}\{(p_1 + p_3)(p_3^* - p_1^*)\} \\ \frac{1}{8h\rho\omega} \text{Im}\{(p_1 + p_4)(p_4^* - p_1^*)\} \end{cases} \quad (\text{A3}) \\
&= \begin{cases} \frac{1}{8h\rho\omega} \text{Im}\{p_1 p_2^* - p_1 p_1^* + p_2 p_2^* - p_2 p_1^*\} \\ \frac{1}{8h\rho\omega} \text{Im}\{p_1 p_3^* - p_1 p_1^* + p_3 p_3^* - p_3 p_1^*\} \\ \frac{1}{8h\rho\omega} \text{Im}\{p_1 p_4^* - p_1 p_1^* + p_4 p_4^* - p_4 p_1^*\} \end{cases} \\
&= \begin{cases} \frac{1}{4h\rho\omega} \text{Im}\{p_1 p_2^*\} \\ \frac{1}{4h\rho\omega} \text{Im}\{p_1 p_3^*\} \\ \frac{1}{4h\rho\omega} \text{Im}\{p_1 p_4^*\}, \end{cases}
\end{aligned}$$

where $2h$ is the separation distance from microphone 1 to the other three microphones and j the imaginary unit.

If instead the pressure estimate of the orthogonal probe is taken to be the pressure of the origin microphone ("1") the intensity is

$$\begin{aligned}
\mathbf{I} &= \begin{cases} I_x \approx \frac{1}{2} \text{Re}\{p_1 v_x^*\} \\ I_y \approx \frac{1}{2} \text{Re}\{p_1 v_y^*\} \\ I_z \approx \frac{1}{2} \text{Re}\{p_1 v_z^*\} \end{cases} \\
&= \begin{cases} \frac{1}{2} \text{Re}\left\{p_1 \left(\frac{j(p_2 - p_1)}{2h\rho\omega}\right)^*\right\} \\ \frac{1}{2} \text{Re}\left\{p_1 \left(\frac{j(p_3 - p_1)}{2h\rho\omega}\right)^*\right\} \\ \frac{1}{2} \text{Re}\left\{p_1 \left(\frac{j(p_4 - p_1)}{2h\rho\omega}\right)^*\right\} \end{cases} \quad (\text{A4}) \\
&= \begin{cases} \frac{1}{4h\rho\omega} \text{Im}\{p_1(p_2^* - p_1^*)\} \\ \frac{1}{4h\rho\omega} \text{Im}\{p_1(p_3^* - p_1^*)\} \\ \frac{1}{4h\rho\omega} \text{Im}\{p_1(p_4^* - p_1^*)\} \end{cases} \\
&= \begin{cases} \frac{1}{4h\rho\omega} \text{Im}\{p_1 p_2^*\} \\ \frac{1}{4h\rho\omega} \text{Im}\{p_1 p_3^*\} \\ \frac{1}{4h\rho\omega} \text{Im}\{p_1 p_4^*\}. \end{cases}
\end{aligned}$$

As Eqs. (A3) and (A4) are equivalent, the two processing methods are equivalent in calculating intensity.

- ¹F. J. Fahy, "Measurement of acoustic intensity using the cross-spectral density of two microphone signals," *J. Acoust. Soc. Am.* **62**, 1057–1059 (1977).
- ²G. Pavic, "Measurement of sound intensity," *J. Sound Vib.* **51**, 533–545 (1977).
- ³J. Y. Chung, "Cross-spectral method of measuring acoustic intensity without error caused by instrument phase mismatch," *J. Acoust. Soc. Am.* **64**, 1613–1616 (1978).
- ⁴H.-E. de Bree, P. Leussink, T. Korthorst, H. Jansen, T. S. J. Lammerink, and M. Elwenspoek, "The μ -flow: A novel device for measuring acoustic flows," *Sens. Actuators A* **54**, 552–557 (1996).
- ⁵F. Jacobsen and H. E. de Bree, "A comparison of two different sound intensity measurement principles," *J. Acoust. Soc. Am.* **118**, 1510–1517 (2005).
- ⁶G. Rasmussen, "Measurement of vector fields," in *Proceedings of the Second International Congress on Acoustic Intensity*, Senlis, France (1985), pp. 53–58.
- ⁷M. Schumacher, "A transducer and processing system to measure total acoustic energy density," M.S. thesis, University of Texas at Austin, Austin, TX, 1984.
- ⁸B. S. Cazzolato and C. H. Hansen, "Errors arising from three-dimensional energy density sensing in one-dimensional sound fields," *J. Sound Vib.* **236**, 375–400 (2000).
- ⁹L. M. C. Santos, C. C. Rodrigues, and J. L. Bento Coelho, "Measuring the three-dimensional acoustic intensity vector with a four-microphone probe," in *Proceedings of Inter-Noise*, Newport Beach, CA (1989), pp. 965–968.
- ¹⁰R. Hickling and A. W. Brown, "Determining the direction to a sound source in air using vector sound-intensity probes," *J. Acoust. Soc. Am.* **129**, 219–224 (2011).
- ¹¹K. L. Gee, J. H. Giraud, J. D. Blotter, and S. D. Sommerfeldt, "Near-field vector intensity measurements of a small solid rocket motor," *J. Acoust. Soc. Am.* **128**, EL69–EL74 (2010).
- ¹²J. W. Parkins, S. D. Sommerfeldt, and J. Tichy, "Error analysis of a practical energy density sensor," *J. Acoust. Soc. Am.* **108**, 211–222 (2000).
- ¹³B. S. Cazzolato and J. Ghan, "Frequency domain expressions for the estimation of time averaged acoustic energy density," *J. Acoust. Soc. Am.* **117**, 3750–3756 (2005).
- ¹⁴J.-C. Pascal and J.-F. Li, "A systematic method to obtain 3D finite-difference formulations for acoustic intensity and other energy quantities," *J. Sound Vib.* **310**, 1093–1111 (2008).
- ¹⁵B. S. Cazzolato and C. H. Hansen, "Errors in the measurement of acoustic energy density in one-dimensional sound fields," *J. Sound Vib.* **236**, 801–831 (2000).
- ¹⁶H. Suzuki, S. Oguro, M. Anzai, and T. Ono, "Performance evaluation of a three dimensional intensity probe," *J. Acoust. Soc. Jpn.* **16**, 233–238 (1995).
- ¹⁷G. W. Elko, "An acoustic vector-field probe with calculable obstacle bias," in *Proceedings of Noise-Con 91*, Tarrytown, NY (1991), pp. 525–532.
- ¹⁸L. L. Locey, "Analysis and comparison of three acoustic energy density probes," M.S. thesis, Brigham Young University, Provo, UT, 2004.
- ¹⁹J. Vandenhout, P. Sas, and R. Snoeys, "Measurement, accuracy and interpretation of real and imaginary intensity patterns in the near field of complex radiators," in *Proceedings of the Second International Congress on Acoustic Intensity*, Senlis, France (1985), pp. 121–128.
- ²⁰K. H. Miah and E. L. Hixson, "Design and performance evaluation of a broadband three dimensional acoustic intensity measuring system," *J. Acoust. Soc. Am.* **127**, 2338–2346 (2010).
- ²¹J. A. Moryl and E. L. Hixson, "A total acoustic energy density sensor with applications to energy density measurement in a reverberation room," in *Proceedings of Inter-Noise*, Beijing, China (1987), pp. 1195–1198.
- ²²P. M. Morse and K. U. Ingard, *Theoretical Acoustics* (McGraw-Hill, New York, 1968), pp. 418–421.
- ²³T. W. Leishman, S. Rollins, and H. M. Smith, "An experimental evaluation of regular polyhedron loudspeakers as omnidirectional sources of sound," *J. Acoust. Soc. Am.* **120**, 1411–1422 (2006).
- ²⁴B. B. Monson, S. D. Sommerfeldt, and K. L. Gee, "Improving compactness for active noise control of a small axial cooling fan," *Noise Control Eng. J.* **55**, 397–407 (2007).
- ²⁵J. R. Oldham, "Development of a multiple microphone probe calibrator," M.S. thesis, Brigham Young University, Provo, UT, 2007.